Journal of Solid State Chemistry 184 (2011) 2966–2971

Contents lists available at SciVerse ScienceDirect

Journal of Solid State Chemistry

journal homepage: www.elsevier.com/locate/jssc

Crystal structures of the novel hydrated borates $Ba_2B_5O_9(OH)$, $Sr_2B_5O_9(OH)$ and $Li_2Sr_8B_{22}O_{41}(OH)_2$

Colin McMillen [a], Carla Heyward [a], Henry Giesber [b], Joseph Kolis [a,*]

[a] Department of Chemistry and Center for Optical Materials Science and Engineering Technologies (COMSET), Clemson University, Clemson, SC 29634, USA
[b] Advanced Photonic Crystals, Fort Mill, SC 29708, USA

ARTICLE INFO

Article history:
Received 21 June 2011
Received in revised form
15 August 2011
Accepted 17 August 2011
Available online 12 September 2011

Keywords:
Hydrothermal
Hydrated borate
Single crystal structure
Alkaline earth borate

ABSTRACT

Three novel hydrated borates $Ba_2B_5O_9(OH)$ (**1**), $Sr_2B_5O_9(OH)$ (**2**) and $Li_2Sr_8B_{22}O_{41}(OH)_2$ (**3**) have been synthesized hydrothermally and their structures determined. Compounds (**1**) and (**2**) are isostructural, crystallizing in space group $P2_1/c$ and having lattice parameters of $a=6.6330(13)$ Å, $b=8.6250(17)$ Å, $c=14.680(3)$ Å, $\beta=93.46(3)^\circ$ and $a=6.4970(13)$ Å, $b=8.4180(17)$ Å, $c=14.177(3)$ Å, $\beta=94.35(3)^\circ$, respectively. Compound (**3**) crystallizes in $P\text{-}1$ with lattice parameters of $a=6.4684(13)$ Å, $b=8.4513(17)$ Å, $c=14.881(3)$ Å, $\alpha=101.21(3)^\circ$, $\beta=93.96(3)^\circ$, $\gamma=90.67(3)^\circ$. While similar in their axis lengths, (**3**) differs greatly in structure and formulation from (**1**) and (**2**). The structure of (**1**) and (**2**) is contrasted to that of the well-known mineral hilgardite ($Ca_2B_5O_9Cl\cdot H_2O$).

1. Introduction

Metal borates have a number of physical properties that make them very intriguing for potential optical applications [1]. They tend to have much wider bandgaps than corresponding phosphates or silicates. In fact many alkali and alkaline earth borates often have band edges near or below 170 nm. They tend to have very high optical damage thresholds and excellent thermal stability. Most importantly they have an increased tendency to crystallize in acentric space groups. Only about 15% of all inorganic crystals grow in acentric space groups whereas over 35% of known borates form acentric crystals making them attractive for use in non-linear optical (NLO) applications [2]. Moreover borates have an exceptionally rich descriptive chemistry. They display two bonding environments, trigonal planar and tetrahedral. These two building blocks are mixed to form an almost infinite variety of rings, chains, frameworks, sheets and mixtures thereof. As a result, the solid-state chemistry of the metal borates is extensive as both naturally formed minerals and synthetic materials [3–5].

These properties of metal borates led to their development as harmonic generators in lasers. In particular their wide bandgaps make them useful in NLO applications in the UV and deep-UV (sub 266 nm) region. The most commonly used crystals for laser manipulations in the UV are β-BaB_2O_4 (BBO) and LiB_3O_5 (LBO) [6,7]. Recently a newer borate $KBe_2(BO_3)F_2$ has garnered considerable attention because of its attractive NLO properties between 266 and 170 nm [8,9].

Because of these important technological properties and their rewarding descriptive chemistry, the synthesis and crystal growth of new metal borates have received considerable attention [1,2,10,11]. The traditional method of metal borate synthesis is through the use of fluxes, which can lead to well-formed crystals. However the flux method has some limitations due to the tendency of borate melts to form glassy products. The amphoteric nature of borates, like the silicates, suggests that the hydrothermal method might be an attractive route to new metal borate crystals. We find that this is indeed the case and a wide variety of new metal borates have been isolated as high quality single crystals. We used the hydrothermal technique to grow optical quality single crystals of several significant NLO crystals such as KBBF [12,13].

In addition a number of new materials have been isolated as single crystals making it clear that the reaction chemistry of the metal borates is still not mined out with an enormous variety of new compounds waiting to be discovered [14,15]. The chemistry of the alkali and alkaline earth borates is proving itself to be very sensitive to the nature and stoichiometry of the metal cation(s). In general the alkali metal cations do not have much of a tendency to become incorporated into the crystal structure with the exception of Li^+, which almost always is incorporated as a part of the structure when it is present in the reaction solution. Unlike the alkali cations, the alkaline earths almost always become part

* Correspondence to: 485 H.L. Hunter Laboratories, Clemson, SC 29634, USA. Fax: 864 656 6613.
E-mail addresses: cmcmill@clemson.edu (C. McMillen), cheywar@clemson.edu (C. Heyward), hgiesber@apcrystal.com (H. Giesber), kjoseph@clemson.edu (J. Kolis).

0022-4596/$ - see front matter © 2011 Elsevier Inc. All rights reserved.
doi:10.1016/j.jssc.2011.08.023

of the chemical formula. In addition the alkaline earth borates are highly sensitive to the stoichiometry, starting materials and synthesis conditions of the reaction. In this paper we describe several new borate compounds that highlight the complexity of the products as well as the sensitivity of the reaction conditions to the starting reagents. In particular we describe several new Sr and Ba borates and contrast them to the product that results when Li^+ is added to the reaction mixture to form a mixed Li/Sr borate. These new results make it clear that the reaction chemistry of hydrothermal borates is continuing to unfold and is certainly not complete yet.

2. Materials and methods

2.1. Hydrothermal synthesis

Crystals of (**1**) and (**2**) were obtained from hydrothermal reactions at 565 °C and 20 kpsi in sealed silver ampoules. Aqueous NaOH (1 M, 0.4 mL) was used as a mineralizer in both cases. The starting charge for (**1**) consisted of 90 mg (0.17 mmol) $(NH_4)_2B_{10}O_{16}\cdot 8H_2O$ (Alfa Aesar, 99.9%) and 40 mg (0.23 mmol) $Ba(OH)_2\cdot H_2O$ (Aldrich, 99.9%). Clear, colorless rods up to 2 mm in size were obtained in approximately 90% yield. A small crystal, $0.20\times 0.08\times 0.08\ mm^3$ in size was selected for single crystal structure determination. Similarly, (**2**) was obtained from a starting charge of 90 mg (0.17 mmol) $(NH_4)_2B_{10}O_{16}\cdot 8H_2O$ (Alfa Aesar, 99.9%) and 61 mg (0.23 mmol) $Sr(OH)_2\cdot 8H_2O$ (Aldrich, 95%). Again, colorless rods up to about 2 mm in size were obtained in about 90% yield. A rod fragment, $0.25\times 0.25\times 0.15\ mm^3$ in size was used for the structure determination.

Crystals of (**3**) were obtained through a two step synthetic process. Feedstock for crystal growth was synthesized from a solid state melt of LiOH (Aldrich, 98+%), B_2O_3 (Alfa Aesar, 97.5%), $Sr(OH)_2\cdot 8H_2O$ (Aldrich, 95%) and KOH (MV Laboratories, 99.99%) in a molar ratio of 2:6:1:3. The powders were thoroughly mixed and heated in a platinum crucible at 900 °C overnight to produce a glass. While potassium is not present in (**3**), KOH was essential in this first step for ensuring that the glass starting material was obtained. Crystals of $Li_2Sr_8B_{22}O_{41}(OH)_2$ were formed by spontaneous nucleation in 0.25″ o.d. silver ampoules using the glass feedstock (0.1 g) and 0.4 mL of 0.5 M LiCl mineralizer solution at 574 °C and 21 kpsi for 7 days. The crystals formed as colorless rods and were the minor product in the hydrothermal reaction, with the majority of the product being $Sr_2B_5O_9(OH)$ (**2**). It is interesting to note that (**3**) was found to only form when using the above glass as a starting material for the hydrothermal reaction and furthermore all attempts to obtain (**3**) without using KOH in this starting material were also unsuccessful.

2.2. Crystal structure determination

Single crystal X-ray diffraction was performed at room temperature using a Rigaku AFC8S diffractometer with graphite monochromated Mo $K\alpha$ radiation ($\lambda=0.71073$ Å) and a Mercury CCD detector. The structures were solved by direct methods and refined by full-matrix least squares on F^2 using the SHELXTL software package [16]. Infrared spectra to corroborate the single crystal structures were obtained using the KBr pellet technique. Samples were analyzed using a Nicolet Magna 550 FTIR spectrometer and data were collected under flowing nitrogen from 400 to 4000 cm^{-1}.

The structure of $Ba_2B_5O_9(OH)$ (**1**) was determined in the monoclinic space group $P2_1/c$ having unit cell parameters of $a=6.6330(13)$ Å, $b=8.6250(17)$ Å, $c=14.680(3)$ Å and $\beta=93.46(3)^\circ$. $Sr_2B_5O_9(OH)$ (**2**) was found to be isostructural with (**1**), having unit cell parameters of $a=6.4970(13)$ Å, $b=8.4180(17)$ Å, $c=14.177(3)$ Å and $\beta=94.35(3)^\circ$. Consecutive refinements resulted in an R-factor of 0.0242 for (**1**) and 0.0272 for (**2**) based on the observed data. All non-hydrogen atoms were refined anisotropically. The hydrogen atoms were assigned by first identifying O10 as a severely underbonded oxygen atom (1.2 v.u.) that was also sterically capable of supporting a hydrogen atom. Residual electron density located about 0.93 Å away from O10 was assigned as the H10 atom, filling out an approximate tetrahedron about O10. H10 was constrained to this distance in accordance with the typical O–H bond distance observed in well-known hydrated borate minerals [17,18]. Table 1 contains crystallographic data for each of the novel hydrated borates in this paper. Selected bond distances and angles of (**1**) and (**2**) are listed in Table 2.

$Li_2Sr_8B_{22}O_{41}(OH)_2$ (**3**) crystallizes in the triclinic system, space group P-1, with $a=6.4684(13)$ Å, $b=8.4513(17)$ Å, $c=14.881(3)$ Å, $\alpha=101.21(3)^\circ$, $\beta=93.96(3)^\circ$, $\gamma=90.67(3)^\circ$. After consecutive refinements, $R_1=0.0477$ based on the observed data. All non-hydrogen atoms were initially refined anisotropically resulting in $R_1=0.0472$ for the observed data. Several atoms (O7, O9, O12, O14, O17, B7, B8, B9, B10, B11) exhibited non-positive definite anisotropic mean square displacements, so additional restraints were placed on these atoms using the ISOR command of SHELXTL in the final refinement, with all others remaining freely anisotropic with no restraints. Several crystals were analyzed by EDX to be sure the observed ADPs of these atoms were not an artifact of potential K/Sr disorder, and to the sensitivity of EDX no K appeared to be present. Crystallographic substitution of Li or K for Sr during test refinements always resulted in higher R_1 values. Any attempts to solve the structure in higher symmetry space groups were unsuccessful, and a structure determination in space group $P1$ contained obvious inversion symmetry

Table 1
Crystallographic data of novel hydrated borates.

	(**1**)	(**2**)	(**3**)
Empirical formula	**$Ba_2B_5O_9(OH)$**	**$Sr_2B_5O_9(OH)$**	**$Li_2Sr_8B_{22}O_{41}(OH)_2$**
Formula weight	489.73	390.30	1642.68
Space group	$P2_1/c$ (no. 14)	$P2_1/c$ (no. 14)	P-1 (no. 2)
a, Å	6.6330 (13)	6.4970 (13)	6.4684 (13)
b, Å	8.6250 (17)	8.4180 (17)	8.4513 (17)
c, Å	14.680 (3)	14.177 (3)	14.881 (3)
α, deg.	90	90	101.21 (3)
β, deg.	93.46 (3)	94.35 (3)	93.96 (3)
γ, deg.	90	90	90.67 (3)
V, Å^3	838.3 (3)	773.1 (3)	795.8 (3)
Z	4	4	1
D_{calc}, mg/m^3	3.880	3.353	3.428
Parameters	156	154	341
μ, mm^{-1}	9.380	13.844	13.46
θ range, deg.	2.74–26.37	2.82–26.34	2.46–25.25
Reflections			
Collected	7752	7256	6962
Independent	1710	1577	2860
Observed [$I\geq 2\sigma(I)$]	1697	1376	2430
R(int)	0.035	0.049	0.0637
Final R (obs. data)[a]			
R_1	0.0242	0.0272	0.0477
wR_2	0.0585	0.0598	0.1150
Final R (all data)			
R_1	0.0246	0.0367	0.0569
wR_2	0.0588	0.0623	0.1214
Goodness of fit on F^2	1.267	1.087	1.04
Largest diff. peak, e/Å^3	1.28	0.85	1.20
Largest diff. hole, e/Å^3	−1.32	−0.66	−2.22

[a] $R_1=[\sum||F_0|-|F_c||]/\sum|F_0|$; $wR_2=\{[\sum w[(F_0)^2-(F_c)^2]^2]\}^{1/2}$.

Table 2
Selected bond distances (Å) and angles (deg.) for $Ba_2B_5O_9(OH)$ (**1**) and $Sr_2B_5O_9(OH)$ (**2**).

Distances	(**1**)	(**2**)	Angles	(**1**)	(**2**)
[BO_3] triangles					
B1–O1	1.356 (6)	1.344 (5)	O1–B1–O2^{9}	124.7 (4)	123.5 (4)
B1–O2^{9}	1.352 (6)	1.359 (5)	O1–B1–O3	115.2 (4)	115.2 (4)
B1–O3	1.390 (6)	1.397 (5)	O2^{1}–B1–O3	120.1 (4)	121.2 (4)
B2–O3^{10}	1.406 (6)	1.413 (6)	O3^{10}–B2–O4	116.6 (4)	116.4 (4)
B2–O4	1.376 (6)	1.376 (5)	O3^{10}–B2–O5^{10}	120.3 (4)	121.4 (4)
B2–O5^{10}	1.331 (6)	1.321 (6)	O4–B2–O5^{10}	123.1 (4)	122.1 (4)
[BO_4] Tetrahedra					
B3–O2	1.547 (5)	1.521 (5)	O2–B3–O7	107.3 (3)	107.0 (3)
B3–O4	1.481 (6)	1.493 (5)	O4–B3–O7	111.3 (4)	110.4 (3)
B3–O6^{7}	1.452 (6)	1.449 (5)	O6^{7}–B3–O7	113.7 (4)	114.2 (4)
B3–O7	1.437 (6)	1.439 (5)			
B4–O7	1.447 (6)	1.447 (5)	O7–B4–O8^{1}	107.6 (4)	106.8 (3)
B4–O8^{1}	1.482 (6)	1.465 (5)	O7–B4–O9^{7}	113.4 (4)	114.2 (3)
B4–O9^{7}	1.468 (6)	1.473 (5)	O7–B4–O10^{6}	109.9 (4)	111.1 (3)
B4–O10^{6}	1.527 (6)	1.530 (5)			
B5–O1^{2}	1.562 (6)	1.560 (5)	O1^{2}–B5–O9	108.5 (4)	109.9 (3)
B5–O6	1.458 (5)	1.463 (5)	O6–B5–O9	113.3 (4)	113.4 (3)
B5–O8	1.450 (6)	1.446 (5)	O8–B5–O9	111.4 (4)	111.7 (3)
B5–O9	1.449 (6)	1.440 (5)			
Alkaline earth (AE) metal polyhedra					
AE1–O1	3.109 (3)	2.840 (3)	AE2–O2	2.837 (3)	2.847 (3)
AE1–O1^{2}	2.801 (3)	2.675 (3)	AE2–O2^{6}	2.736 (3)	2.646 (3)
AE1–O3	2.669 (4)	2.548 (3)	AE2–O5	2.767 (3)	2.542 (3)
AE1–O4^{11}	2.683 (3)	2.519 (3)	AE2–O5^{6}	2.846 (4)	2.639 (3)
AE1–O5^{5}	2.868 (4)	2.735 (3)	AE2–O6	2.752 (3)	2.605 (3)
AE1–O6	2.870 (3)	2.780 (3)	AE2–O7	2.755 (3)	2.658 (3)
AE1–O8	3.046 (4)	2.693 (3)	AE2–O8^{1}	2.791 (3)	2.644 (3)
AE1–O9^{8}	2.618 (3)	2.520 (3)	AE2–O9^{8}	3.008 (3)	2.937 (3)
AE1–O10	2.668 (4)	2.511 (3)	AE2–O10^{3}	2.913 (4)	2.876 (3)

Symmetry codes: (1) $x-1$, y, z; (2) $-x+1$, $-y$, $-z+1$; (3) $-x+1$, $y-1/2$, $-z+3/2$; (4) $x-1$, $-y+1/2$, $z+1/2$; (5) $x+1$, y, z; (6) $-x$, $y-1/2$, $-z+3/2$; (7) $-x$, $y+1/2$, $-z+3/2$; (8) $-x+1$, $y+1/2$, $-z+3/2$; (9) x, $-y+1/2$, $z-1/2$; (10) x, $-y+1/2$, $z+1/2$; (11) $x+1$, $-y+1/2$, $z-1/2$.

and was converted to space group *P*-1. Thus it appears the observed anisotropic displacements and larger e.s.d. values in the case of (**3**) are an artifact of lower crystal quality (and a small selection of crystals). The unique hydrogen atom was assigned to O10 again by identifying this oxygen atom as underbonded (1.14 v.u.). The location of this hydrogen atom was identified as residual electron density 1.02 Å away from O10. Bond distance and angle data for (**3**) is listed in Table 3.

3. Results and discussion

3.1. Structures of $Ba_2B_5O_9(OH)$ (*1*) and $Sr_2B_5O_9(OH)$ (*2*)

The structure of (**1**) and (**2**) contains two triangular and three tetrahedral borate units with average B–O bond distances in both compounds of 1.37 Å and 1.48 Å for the triangular and tetrahedral groups, respectively. These values are in good agreement with accepted values of 1.37 Å and 1.46 Å reported in the literature [4]. A closer look at the tetrahedral borates reveals that they are each noticeably distorted in one of their B–O bond distances. In the B3 and B5 tetrahedra this distortion involves an oxygen atom that bridges the tetrahedral boron with a triangularly coordinated boron atom. In these cases the triangular boron contributes a greater valence toward the oxygen atom, pulling it farther away from the tetrahedral boron. In a final case (B4), the B–O distance is lengthened because of a reduced attractive force between the boron atom and a protonated oxygen atom (O10).

Table 3
Selected bond distances (Å) and angles (deg.) for $Li_2Sr_8B_{22}O_{41}(OH)_2$ (**3**).

Distances	(**3**)	Angles	(**3**)
[BO3] triangles			
B1–O1	1.349(11)	O1–B1–O2	123.3(7)
B1–O2	1.353(9)	O1–B1–O3	115.4(6)
B1–O3	1.392(11)	O2–B1–O3	121.3(7)
B2–O3^{11}	1.414(11)	O3^{11}–B2–O4	123.1(7)
B2–O4	1.305(11)	O3^{11}–B2–O5	114.4(7)
B2–O5	1.390(9)	O4–B2–O5	122.4(7)
B9–O15^{8}	1.334(8)	O15^{8}–B9–O17	120.7(7)
B9–O17	1.399(9)	O15^{8}–B9–O18	120.8(7)
B9–O18	1.380(10)	O17–B9–O18	118.5(6)
B10–O16	1.363(9)	O16–B10–O18^{8}	122.9(7)
B10–O18^{8}	1.385(10)	O16–B10–O19^{1}	121.0(7)
B10–O19^{1}	1.365(10)	O18^{8}–B10–O19^{1}	116.1(6)
B11–O20	1.327(10)	O20–B11–O21	125.5(6)
B11–O21	1.363(10)	O20–B11–O22	118.1(6)
B11–O22	1.413(7)	O21–B11–O22	116.4(6)
[BO_4] Tetrahedra			
B3–O2	1.528(10)	O7–B3–O6	113.6 (6)
B3–O5^{11}	1.470(10)	O7–B3–O5^{11}	111.3 (6)
B3–O6	1.467(9)	O7–B3–O2	107.6 (6)
B3–O7	1.436(9)		
B4–O1^{1}	1.545(10)	O1^{1}–B4–O6	103.4(5)
B4–O6	1.454(9)	O1^{1}–B4–O8^{1}	107.0(6)
B4–O8^{1}	1.461(8)	O1^{1}–B4–O9	110.7(6)
B4–O9	1.444(8)		
B5–O7^{2}	1.450(9)	O7^{2}–B5–O9^{2}	113.4 (5)
B5–O9^{2}	1.474(8)	O7^{2}–B5–O11	107.0 (6)
B5–O10	1.524(9)	O7^{2}–B5–O10	111.6 (6)
B5–O11	1.474(10)		
B6–O11	1.431(8)	O11–B6–O13	112.9 (5)
B6–O12	1.464(9)	O11–B6–O12	111.0 (6)
B6–O13	1.431(8)	O11–B6–O19	107.7 (6)
B6–O19	1.574(10)		
B7–O8^{4}	1.453(9)	O8^{4}–B7–O13	111.7 (5)
B7–O13	1.462(8)	O8^{4}–B7–O14	106.3 (6)
B7–O14	1.464(8)	O8^{4}–B7–O17^{5}	110.1 (5)
B7–O17^{5}	1.536(9)		
B8–O12	1.454(8)	O12–B8–O14	114.0 (5)
B8–O14	1.456(8)	O12–B8–O16	107.1 (6)
B8–O15	1.494(9)	O12–B8–O15	109.0 (5)
B8–O16	1.483(9)		
[LiO_5] polyhedron			
Li1–O14^{9}	1.945(13)	O14^{9}–Li1–O20^{10}	114.1(6)
Li1–O15	1.916(14)	O15–Li1–O20^{10}	110.8(7)
Li1–O18^{10}	2.455(14)	O15–Li1–O19	90.7(6)
Li1–O19	2.016(13)	O19–Li1–O14^{10}	138.7(7)
Li1–O20^{10}	1.937(13)	O15–Li1–O18^{10}	149.2(6)
[SrO_9] and [SrO_{10}] polyhedra			
Sr1–O2	2.790(5)	Sr2–O1^{4}	2.634(4)
Sr1–O4	2.708(5)	Sr2–O1^{3}	2.834(5)
Sr1–O7	2.633(6)	Sr2–O3^{3}	2.541(5)
Sr1–O9^{2}	2.937(5)	Sr2–O4	2.715(5)
Sr1–O10	2.913(5)	Sr2–O5	2.501(6)
Sr1–O11^{1}	2.608(5)	Sr2–O6^{5}	2.807(5)
Sr1–O12	2.583(5)	Sr2–O8^{4}	2.748(5)
Sr1–O16	2.650(5)	Sr2–O10	2.508(5)
Sr1–O21	2.546(5)	Sr2–O13	2.493(5)
Sr3–O2	2.670(5)	Sr4–O9	2.525(5)
Sr3–O4^{6}	2.584(5)	Sr4–O11^{1}	2.745(5)
Sr3–O6	2.600(5)	Sr4–O12^{1}	2.786(5)
Sr3–O8	2.652(5)	Sr4–O17	2.618(4)
Sr3–O13^{7}	2.934(5)	Sr4–O19^{1}	2.727(5)
Sr3–O14^{6}	2.688(5)	Sr4–O20^{1}	2.503(5)
Sr3–O16^{6}	2.901(5)	Sr4–O20^{8}	2.583(6)
Sr3–O17	2.747(4)	Sr4–O21	2.676(6)
Sr3–O18	3.217(5)	Sr4–O22	2.845(1)
Sr3–O21	2.667(5)		

Symmetry codes: (1) $x-1$, y, z; (2) $x+1$, y, z; (3) $-x+1$, $-y$, $-z$; (4) x, $y+1$, z; (5) $x+1$, $y+1$, z; (6) x, $y-1$, z; (7) $x-1$, $y-1$, z; (8) $-x$, $-y$, $-z+1$; (9) $-x+1$, $-y+1$, $-z+1$; (10) $-x+1$, $-y$, $-z+1$; (11) $-x$, $-y$, $-z$.

While these materials resemble hilgardite-type compounds ($Ca_2B_5O_9Cl \cdot H_2O$) in their composition and number of triangular and tetrahedral borate units, slight differences in the borate fundamental building block (FBB) differentiate the two structures. [19–21] The FBB of (**1**) and (**2**) consist of two approximately orthogonal interlocking rings sharing a common borate tetrahedron, forming a $[B_5O_{11}(OH)]^{8-}$ unit. This is shown in Fig. 1a which pictures the extended asymmetric unit as 50% probability thermal ellipsoids. Using the notation developed by Hawthorne et al. [4], this building block can be expressed as $\langle 2\Delta\square\rangle$–$\langle 3\square\rangle$, indicating that the interlocking rings are non-identical. This differs from the hilgardite structure that has the classical pentaborate $[B_5O_{12}]^{9-}$ building block (Fig. 1b) consisting of two identical rings $\langle\Delta 2\square\rangle$–$\langle\Delta 2\square\rangle$. The primary differences are observed at the B1 and B5 positions.

The slightly different ring structures lead to a different overall polymerization of the building blocks. In hilgardite, infinite chains of building blocks are connected in all directions to form a zeolite-like framework, whereas chains of $[B_5O_{11}(OH)]^{8-}$ groups in (**1**) and (**2**) are connected only along the *a* and *b* axes. Chain connectivity occurs along [1 0 0] through B1–O1–B5 and B5–O6–B3 linkages where B1 is triangular and B3 and B5 are tetrahedral units. Connectivity by B4–O8–B5 tetrahedral borate linkages forms the chain structure along [0 1 0]. In concert these chains form sheets that are connected to neighboring sheets along the *c*-axis by Ba or Sr atoms, not through B–O bonding (as in hilgardite). In connecting the sheets, the unique alkaline earth metals are both 9-coordinate with oxygen, having bond distances ranging from 2.618(3) to 3.109(3) Å for Ba–O bonds and 2.511(3)–2.840(3) Å for Sr–O bonds. In spite of these substantial structural differences, the borate network of (**1**) and (**2**) exhibits voids along the *a* and *b* axes similar to the framework of hilgardite (Fig. 2). Alkaline earth metal atoms reside in the channels along the *b*-axis, while the hydrogen atom of the FBB extends into the voids along the *a*-axis. There appears to be no extended hydrogen bonding in the structure of (**1**) and (**2**) since there are no other oxygen atoms within a reasonable distance of the hydrogen atoms in these voids.

Infrared spectroscopy was used to verify the nature of the borate groups and the presence of hydroxide in the structure. Three main bands are visible in the spectrum shown in Fig. 3. The B–O asymmetric stretching vibrations are the most prominent vibrational modes in the infrared spectra of borates. The bands at 1394 cm^{-1} corresponds to triangular borate groups in the presence of tetrahedral borate groups, while the bands centered at 930 cm^{-1} arises from tetrahedral borate groups in the presence of triangular borates. [22,23] The presence of the hydroxide group is confirmed by the broad absorption band at 3453 cm^{-1}.

3.2. Structure of $Li_2Sr_8B_{22}O_{41}(OH)_2$

At first glance, $Sr_2B_5O_9(OH)$ and $Li_2Sr_8B_{22}O_{41}(OH)_2$ appear to have similar lattice parameters, suggesting they may also possess

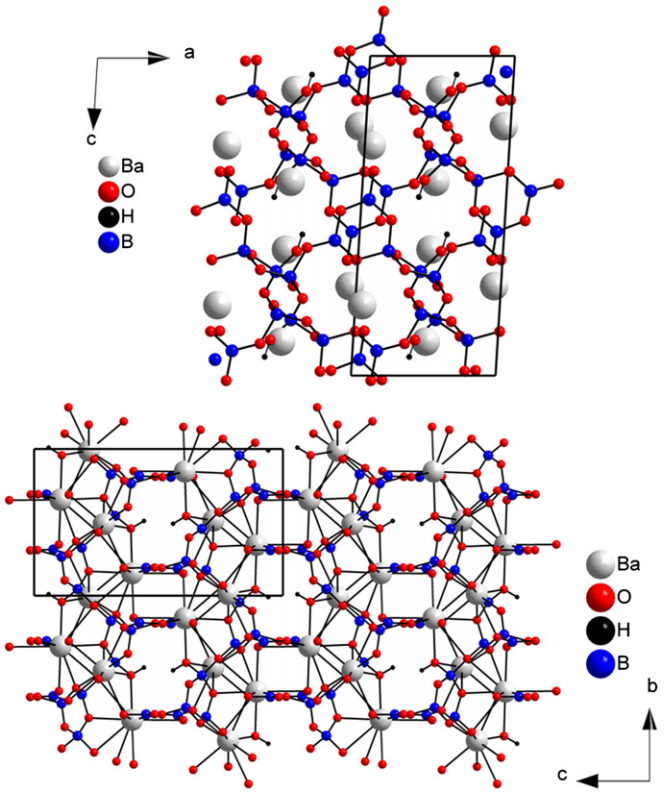

Fig. 2. $Ba_2B_5O_9(OH)$ structure viewed along [0 1 0] (top) and [1 0 0] (bottom).

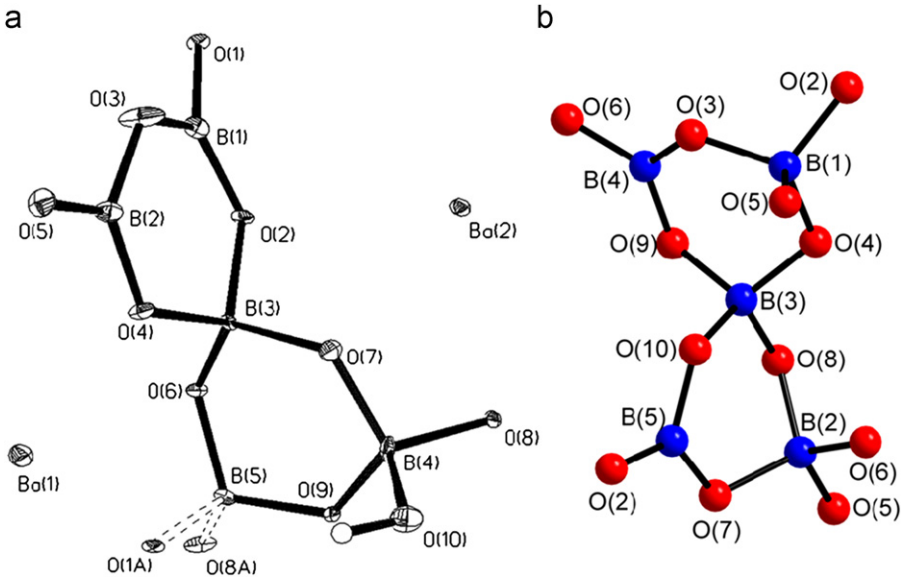

Fig. 1. (a) Extended asymmetric unit of (**1**) and (**2**) (as 50% probability thermal ellipsoids for $Ba_2B_5O_9(OH)$). (b) $(B_5O_{12})^{9-}$ polyanion of hilgardite (after ref [19]).

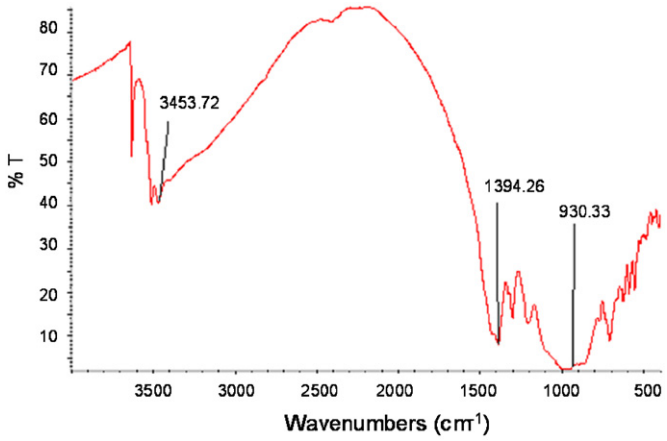

Fig. 3. Representative IR spectrum ($Ba_2B_5O_9(OH)$) of (**1**) and (**2**).

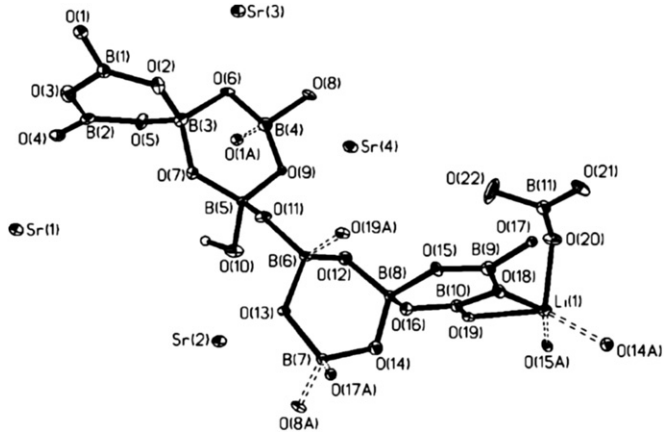

Fig. 4. Extended asymmetric unit of (**3**) as 50% thermal ellipsoids.

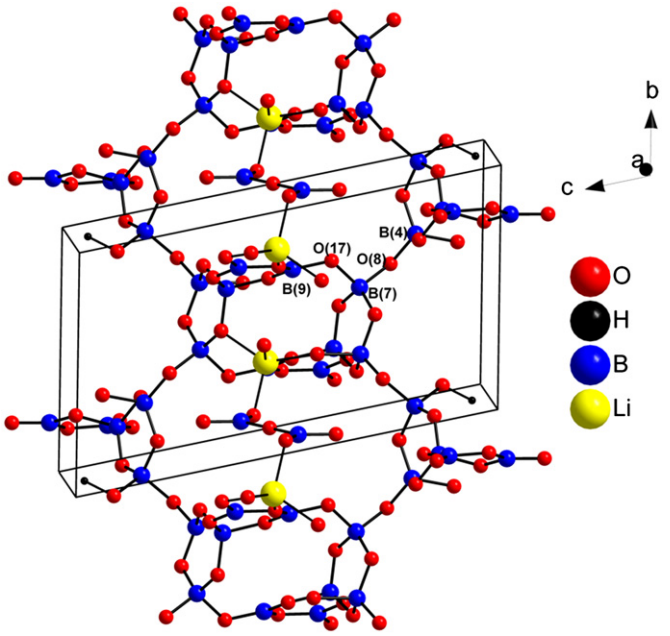

Fig. 5. Lithium borate framework of (**3**) viewed off [1 0 0] (Sr atoms omitted for clarity).

significant structural similarities. However, their symmetries are very different and the two compounds are comprised of borate building blocks that do differ greatly from one another so the structures are easily distinguished. The structure of $Li_2Sr_8B_{22}O_{41}(OH)_2$ is composed of an unusually complex $[B_{10}O_{19}(OH)]^{-9}$ unit, a stand-alone $[B_2O_5]^{4-}$ group, four unique strontium atoms, and one unique lithium atom. These are shown as thermal ellipsoids in Fig. 4. The FBB in this structure is a $[B_{10}O_{19}(OH)]^{-9}$ unit that consists of six BO_4 groups and four BO_3 groups forming two pairs of orthogonal interlocking rings with O11 bridging the pairs. The FBB can be written as $\langle 2\Delta\square\rangle - \langle 3\square\rangle\langle 3\square\rangle - \langle 2\Delta\square\rangle$ according to the notation given by Hawthorne et al. [4] While the first half of this FBB (containing B1 through B5) is similar to the FBB of (**1**) and (**2**), the second half of the FBB (containing B6 through B10) is distinguished in that it does not possess a protonated oxygen atom.

The average BO_3 and BO_4 bond distances are close to their expected values, 1.368 and 1.476 Å, respectively. Slightly elongated tetrahedral B–O bond distances are observed for B4–O1 (1.545 (10) Å), B6–O19 (1.574 (10) Å) and B7–O17 (1.536 (9) Å), where these O atoms link to three-coordinate B atoms in neighboring FBBs. B5–O10 is also slightly elongated (1.524 (9) Å), as O10 is the protonated oxygen in the structure. Connectivity of the $[B_{10}O_{19}(OH)]^{-9}$ units occurs through the elongated B–O bonds connecting three and four-coordinate boron atoms: B1–O1–B4 (along [1 0 0]), B6–O19–B10 (along [1 0 0]) and B7–O17–B9 (along [0 0 1]). Linkages also occur through B4–O8–B7 bonds (generally along [0 1 0]), where both B4 and B7 are both tetrahedral boron atoms.

Structural connections also occur through Li bonding with O15, O19, O14 and O18 to continue the framework structure. This complex framework exhibits voids in which B_2O_5 (pyroborate) groups lie. The full lithium borate framework including these pyroborates is shown in Fig. 5. These pyroborate groups are comprised of two B11 triangular boron atoms sharing O22. The terminal oxygens O20 and O21 are 1.327(10) and 1.363(10) Å away from B11 while the length of the bridging oxygen O22 is slightly longer at 1.413(7) Å. The small elongation in the bridging oxygen is typical for pyroborate anions. [24] The angles of O20–B11–O21, O21–B11–O22, and O20–B11–O22 all total to 360° which supports the planarity of the B_2O_5 group. The Li atom connects the pyroborate to the rest of the framework through O18–Li1–O20 and O19–Li1–O20 bonding. The LiO_5 polyhedron is a severely distorted trigonal bipyramid due to one especially long bond (2.455(14) Å), Li1–O18, opposite Li1–O15 which at 1.916(14) Å is a more typical Li–O bond distance. There is also some angular distortion in these axial atoms (O15–Li1–O18 = 149.2°) as well as in the equatorial atoms where O14–Li1–O20 is 114.1°, O20–Li1–O19 is 102.0° and O19–Li1–O14 is 138.7° rather than an idealized 120°. This structure consists of both nine- and ten-coordinate Sr atoms. The nine and ten coordinate Sr–O bond distances vary from 2.501(6)–2.937(5) Å and 2.584(5)–3.217(5) Å, respectively. These Sr–O bonds provide further connectivity between the pyroborate groups and the FBB as well as connecting the FBB to adjacent FBBs. Unfortunately due to the presence of (**3**) as only a minor reaction product with (**2**), sufficient pure material for IR analysis was not obtained even after successive synthetic reactions.

4. Conclusions

In our effort to expand the exploratory descriptive chemistry of the *s*-block metal borates several new alkaline earth metal borates have been prepared in hydrothermal synthesis conditions. As amphoteric oxides the borates show good reactivity in basic solution, forming stable crystals of new materials. The use

of alkaline earths in the starting charge in these hydrothermal systems most commonly leads to the incorporation of the alkaline earth ion as an integral part of the structure whereas alkali metals in the mineralizer typically act as spectator ions as observed in $Sr_2B_5O_9(OH)$ and $Ba_2B_5O_9(OH)$ in this study. The obvious exception is the Li^+ ion which has a significant effect on the chemistry, as demonstrated here in the complex product $Li_2Sr_8B_{22}O_{41}(OH)_2$. It is clear that mixtures of Li^+ and alkaline earth cations provide a route to a whole new class of new compounds and structure types. The materials reported here do not crystallize in acentric space groups, precluding them from use in NLO applications. Furthermore the presence of OH^- groups in the lattice is unsatisfactory due to their tendency to dehydrate upon heating. Further exploratory work is underway to synthesize new acentric products by varying the reactions conditions and also eliminate the presence of OH^- groups in the crystalline lattice. These results are the subject of forthcoming reports.

Acknowledgment

We are indebted to the National Science Foundation for their support of this work (DMR-0907359).

Appendix A. Supplementary Material

Supplementary data associated with this article can be found in the online version at doi:10.1016/j.jssc.2011.08.023.

References

[1] D.A. Keszler, Curr. Opin. Sol. State Mater. Sci. 1 (1996) 204.
[2] P. Becker, Adv. Mater. 10 (1998) 979.
[3] G. Heller, Topics Curr. Chem. 131 (1986) 39.
[4] F.C. Hawthorne, P.C. Burns, J.D. Grice, Crystal Chemistry of Boron, in: E.S. Grew, L.M. Anovitz (Eds.), Reviews in Mineralogy Volume 33: Boron—Mineralogy, Petrology and Geochemistry, Mineralogical Society of America, Washington, D.C, 2002, pp. 41–116.
[5] C.L. Christ, J.R. Clark, Phys. Chem. Miner. 2 (1977) 59.
[6] C. Chen, B. Wu, A. Jiang, G. You, Sci. Sin. B 28 (1985) 235.
[7] C. Chen, Y. Wu, A. Jiang, G. You, R. Li, S. Lin, J. Opt. Soc. Am. B 6 (1989) 616.
[8] L. Mei, Y. Wang, C. Chen, B. Wu, J. Appl. Phys. 74 (1993) 7014.
[9] C.T. Chen, G.L. Wang, X.Y. Wang, Z.Y. Xu, Appl. Phys. B 97 (2009) 9.
[10] T. Sasaki, Y. Mori, M. Yoshimura, K.Y. Yoke, T. Kamimura, Mater. Sci. Eng. 30 (2000) 1.
[11] C. Chen, Z. Lin, Z. Wang, Appl. Phys. B 80 (2005) 1.
[12] C.D. McMillen, J.W. Kolis, J. Cryst. Growth 310 (2008) 2033.
[13] C.D. McMillen, J. Hu, D. VanDerveer, J.W. Kolis, Acta Cryst. B 65 (2009) 445.
[14] J.W. Kolis, C.D. McMillen, T. Franco, Mater. Res. Soc. Symp. Proc 848 (2005) 3.
[15] C.D. McMillen, J.W. Kolis, Inorg. Chem. 50 (2011) 6809–6813.
[16] G.M. Sheldrick, Acta Cryst. A 64 (2008) 112.
[17] P.C. Burns, F.C. Hawthorne, Can. Miner. 31 (1993) 297.
[18] P.C. Burns, F.C. Hawthorne, Can. Miner. 32 (1994) 895.
[19] P.C. Burns, F.C. Hawthorne, Acta Cryst. C 50 (1994) 653.
[20] J. Barbier, H. Park, Can. Miner. 39 (2001) 129.
[21] B.V. Egorova, A.V. Olenev, P.S. Berdonosov, A.N. Kuznetsov, S.Y. Stefanovich, V.A. Dogikh, T. Mahenthirarajah, P. Lightfoot, J. Solid State Chem. 181 (2008) 1891.
[22] S.D. Ross, Borates, in: V.C. Farmer (Ed.), Mineralogical Society Monograph 4: The Infrared Spectra of Minerals, Mineralogical Society, London, 1974, pp. 205–226.
[23] C.E. Weir, J. Res. Natn. Bur. Stand 70A (1966) 153.
[24] P.D. Thompson, J. Huang, R. Smith, D. Keszler, J. Solid State Chem. 95 (1991) 126.